Pigeons Steer Like Helicopters and Generate Down- and Upstroke Lift During Low Speed Turns

TITLE PAGE.

Classification. Biological Sciences. Biophysics and Computational Biology.

Title. Pigeons steer like helicopters and generate down- and upstroke lift during low speed turns.

Authors. Ivo G. Ros[1], Lori C. Bassman[2], Marc A. Badger[2], Alyssa N. Pierson[2] and Andrew A. Biewener[1]

Author affiliation. [1]Harvard University, Department of Organismic and Evolutionary Biology, Concord Field Station, 100 Old Causeway Road, Bedford, MA 01730, USA

[2]Harvey Mudd College, Department of Engineering, 301 Platt Blvd., Claremont, CA 91711, USA

Corresponding author. Ivo G. Ros, 100 Old Causeway Road, Bedford, MA 01730

Phone: 626.731.4103; Fax: 781.275.9613; Email: Ivo.Ros@gmail.com

ABSTRACT. Turning is crucial for animals, particularly during predator-prey interactions and to avoid obstacles. For flying animals, turning consists of changes in 1) flight trajectory, or path of travel, and 2) body orientation, or 3D angular position. Changes in flight trajectory can only be achieved by modulating aerodynamic forces relative to gravity. How birds coordinate aerodynamic force production relative to changes in body orientation during turns is key to understanding the control strategies used in avian maneuvering flight. We hypothesized that pigeons produce aerodynamic forces in a uniform direction relative to their body, requiring changes in body orientation to redirect those forces to turn. Using detailed 3D kinematics and body mass distributions, we examined net aerodynamic forces and body orientations in slowly flying pigeons (*Columba livia*) executing level 90º turns. The net aerodynamic force averaged over the downstroke was maintained in a fixed direction relative to the body throughout the turn, even though the body orientation of the birds varied substantially. Early in the turn, changes in body orientation primarily redirected the downstroke aerodynamic force, affecting the bird's flight trajectory. Subsequently, the pigeons mainly reacquired the body orientation used in forward flight without affecting their flight trajectory. Surprisingly, the pigeon's upstroke generated aerodynamic forces that were approximately 50% of those generated during the downstroke, nearly matching the relative upstroke forces produced by hummingbirds. Thus, pigeons achieve low speed turns much like helicopters, by using whole-body rotations to alter the direction of aerodynamic force production to change their flight trajectory.

Keywords: Maneuvering; Flight; Biomechanics; Tip-reversal; Pigeon

\body

INTRODUCTION. Maneuverability is critical to the movement of animals in their natural environment. Turning represents a basic maneuver that is particularly relevant to predator-prey interactions and obstacle avoidance. To begin to understand the mechanisms by which birds achieve and control aerial turns, we examine the role of body rotations in relation to aerodynamic force production to alter the flight *trajectory*, or path of travel, during turns. More specifically, we ask whether body rotations serve to redirect aerodynamic forces during low speed 90° level turns in pigeons.

The three dimensional (3D) nature of flight requires analyses of aerodynamic force production in relation to body motions not only in a global reference frame, but also in a local, body reference frame (Fig. 1). The global frame allows for application of Newton's laws of motion, which for a flying bird means that the resultant of aerodynamic and gravitational forces can be estimated from accelerations of the whole body center of mass (CM). However, the bird's torso moves relative to the CM, primarily due to the time-varying wing configurations during the wingbeat cycle. Therefore, localization of the CM cannot rely solely on the torso, but requires detailed assessment of the motions of the head and wings as well. The body frame corrects for the displacements and rotations of the torso, allowing for analyses of head and wing motions and forces relative to the body, which subsequently can be related to underlying musculoskeletal and sensory-motor function. The combination of global and local frames therefore can reveal how aerodynamic force production is coordinated with a bird's 3D *body orientation*, or body angular position, during aerial turns.

There are two major reasons for animals to change their body orientations during turns: 1) to reacquire their preferred body orientation for forward movement, and 2) to alter the direction of propulsive force needed to change their movement trajectory. Bilaterally symmetric animals have body plans that are best suited for forward locomotion with a particular 3D body orientation (1). Consequently, this preferred body orientation must be reacquired during a turn to move along the new movement trajectory. Additionally, body rotations must also occur to redirect the animal's propulsive turning forces, if these forces are directionally constrained within the animal's body frame. Redirecting resultant forces in the global frame due to changes in body orientation is referred to as *force vectoring* (Figure 1). In fact, flying insects have been argued to turn primarily by force vectoring, meaning that the majority of the redirection of aerodynamic forces is based on changes in body orientation, and not on changes in the direction of aerodynamic forces relative to the insect's body (2).

Even though quantifying the time-varying aerodynamic forces produced during flapping flight is challenging, estimates of aerodynamic force production during flight maneuvers have been made in insects (4-7). Turning calliphorid, muscid and drosopholid flies support the use of force vectoring as a means to redirect aerodynamic force, as the aerodynamic forces produced by their wings operate within a limited range relative to their bodies. Most of the redirection of aerodynamic force within the body frame occurs within the animal's mid-sagittal plane, varying over a range of merely 20°; although fruit flies also generate moderate lateral forces with respect to their body. Notable exceptions are hover flies (Syrphidae), which seem to achieve a wider variation in aerodynamic

force orientation relative to their body (8, 9), though these findings have been questioned (7).

Vertebrate fliers also appear to have a limited ability to redirect aerodynamic force relative to their body. Horseshoe bats, fruit bats, pigeons and rose-breasted cockatoos roll during aerial turns (10-13), indicating that they likely rely on force vectoring to turn. Fruit bats rotate their bodies in the direction of the turn in addition to rolling, increasing their centripetal acceleration (13). Finally, pigeons appear to redirect aerodynamic forces to accelerate after flight take-off and brake prior to landing by pitching movements of their bodies (14).

Here, we ask whether pigeons redirect aerodynamic forces (in the global frame) by redirecting aerodynamic forces relative to their body (Fig. 1A), or by rotating the body itself (Fig. 1B). Given the constrained musculoskeletal and stereotypical kinematic features of the avian wingstroke (15-18), we hypothesize that pigeons generate aerodynamic forces in a uniform direction relative to their body (*i.e.* in the body frame), necessitating the use of force vectoring to turn (Fig. 1B). To test this hypothesis, we used high-speed videography to obtain 3D positions of body markers of pigeons performing low speed, 90º level turns within a netted, 10m long, square-corner corridor (Fig. 2). Detailed analysis of the pigeons' whole-body mass distributions enabled their non-body-fixed CM to be accurately tracked, from which time-varying, whole-body, or net, aerodynamic forces were assessed (Fig. 2-5). To interpret the functional significance of changes in body orientation made throughout the turn, body rotations of the pigeons were quantified relative to the redirection of aerodynamic force averaged over successive downstrokes. Specifically, for each downstroke in the turn the component of the body

rotation that redirected the average aerodynamic force was mathematically separated from the component of the 3D body rotation that had no effect on the direction of the average downstroke force. This approach allowed any 3D body rotation to be decomposed into two complementary body rotation fractions, one that redirected and one that rotated about the downstroke average aerodynamic force (Fig. 6).

RESULTS. Three pigeons with a mean body mass of 319 $\pm$ 33 g (all results are expressed as mean $\pm$ SD) negotiated the 90° level turn at a CM speed of 3.3 $\pm$ 0.2 ms^{-1}, with mean flight trajectory slopes relative to the global horizontal plane of 2.5 $\pm$ 0.2^{o}, and a wingbeat frequency of 8.3 $\pm$ 0.3 Hz. Combined wing mass distal to the shoulder comprised 12.5 $\pm$ 1.4% of total body mass.

Aerodynamic forces are reaction forces resulting from the interactions of the animal's body, wings and tail with the surrounding air. In mid-air, an animal's flight trajectory can only be changed by gravity or the aerodynamic forces produced by the animal. Since the external force on an object equals the product of its mass and acceleration, the instantaneous aerodynamic force acting on the pigeon's center of mass (CM) can be estimated after factoring out gravity (see methods for details). However, the time-varying configurations of the bird's wings and head relative to its torso cause the whole-body, or net, CM to vary in position with respect to the torso through time. This non-body-fixed CM therefore requires estimates based on detailed 3D kinematics and body mass distributions (Fig. 3). Using a mass-distribution model then provides estimates of instantaneous net aerodynamic forces (**F**) throughout the turns. The aerodynamic

130 origin of these forces and any force components that cancel out internally, however,
131 cannot be identified by this method.

132 **Pigeons turn with an aerodynamically active upstroke.** Throughout the 90^{o}
133 turn the pigeons produced aerodynamic forces during the upstroke as well as the
134 downstroke (Fig. 2, 4). In the global frame, aerodynamic forces were directed vertically
135 to support the pigeon's body weight and horizontally to change its flight trajectory during
136 the turn (Fig. 2).

137 **Substantial body rotations occur about all three anatomical axes.** The 3D
138 body rotations of the turning pigeons consisted of substantial roll, pitch and yaw
139 components, defined as rotations about the antero-posterior (along the spine), the medio-
140 lateral and dorso-ventral body frame axes, respectively (19) (Table 1; Fig. 1). During the
141 turn, body rotations oscillated back and forth within wingbeats, but led to net changes in
142 body orientation between successive wingbeats. The pigeons' 3D body rotations
143 predominantly consisted of roll, both continuously and on a net wingbeat basis; although
144 pitch and yaw components were also substantial (Table 1). Over the course of a turn,
145 early wingbeats rolled the pigeons into the turn, with subsequent wingbeats producing net
146 roll rotations out of the turn. In contrast, net wingbeat rotations about the pitch and yaw
147 axes were directed upwards and into the turn, respectively, throughout turning.
148 Oscillations of body rotations within wingbeats were larger in pitch and roll (16 ± 5 and
149 13 ± 6 °/wingbeat, respectively), and smallest in yaw (4 ± 3 °/wingbeat), indicating yaw
150 angular velocities were most uniform

151 **Pigeons produce consistent patterns of aerodynamic force.** The directions and
152 magnitudes of instantaneous net aerodynamic force (**F**) exhibited stereotypic patterns

within the body frame during both downstroke and upstroke. (Fig. 2D, 4, 5). During downtroke **F** was directed mainly in the midsagittal plane of the birds, whereas during upstroke **F** was more variably directed. Net aerodynamic force magnitude (|**F**|) approximated zero at the upstroke-downstroke transition, before peaking near mid-downstroke (4.5 $\pm$ 0.4 body weights (BW) at 53% of the downstroke period; Fig. 4). At the downstroke-upstroke transition, **F** momentarily opposed the stroke average. Throughout the remainder of the upstroke, however, the pigeons produced aerodynamic force in support of body weight, in line with the stroke average. |**F**| reached a maximum at mid-upstroke (2.3 $\pm$ 0.3 BW, Fig. 4), coinciding with tip-reversal (Fig. 4B, left silhouette). Although upstroke peak |**F**| averaged about half the downstroke peak |**F**|, the aerodynamic impulse generated during upstroke averaged 27 $\pm$ 4% of the impulse generated during downstroke. Aerodynamic forces averaged 1.33 $\pm$ 0.07 BW over the full wingbeat cycle, consistent with the pigeons' need for centripetal forces in addition to weight support to fly through the turn. A sensitivity analysis consisting of a decrease and an increase of the wing masses by 10% resulted in an increase and a decrease of upstroke peak force estimate by approximately 5%, respectively, indicating the robustness of our findings for upstroke aerodynamic force based on a full body and wing mass distribution model of the birds.

As the pigeon rotated its body and changed its flight trajectory, downstroke-averaged aerodynamic forces ($\mathbf{F}_d$) were produced in a uniform direction with respect to the pigeon's body during the five sequential wingbeats of the turn (Fig. 5). $\mathbf{F}_d$ were oriented in the mid-sagittal plane of the bird's body and directed anterior to the dorso-ventral body axis by 38 + 7° (Fig. 5), consistent with the 'pitched-up' body orientation of

pigeons during slow steady flight (~ 32° at a flight speed of 5-6 ms^{-1} (20)). During slow flight aerodynamic drag is small and, by approximation, only gravity needs to be countered by near vertical aerodynamic forces.

Turning pigeons prioritize changes in trajectory over angular positioning of the body. By comparing rotations of the pigeon's torso with respect to redirection of $\mathbf{F}_d$ over the course of a wingbeat in the global frame, we evaluated the extent to which pigeons relied on body rotations to redirect $\mathbf{F}_d$ versus to what extent body rotations occurred about the direction of $\mathbf{F}_d$ (see methods for details). Body rotations that redirect $\mathbf{F}_d$ alter flight trajectory, but body rotations about $\mathbf{F}_d$ leave the direction of $\mathbf{F}_d$ in the global frame unaffected, and therefore do not change flight trajectory. This analysis revealed that for each sequential wingbeat of the turn, the pigeon's body progressively rotated about an axis that was increasingly aligned with the direction of $\mathbf{F}_d$ (Fig. 6). Body rotations produced over the course of the first two wingbeats of the turn predominantly redirected $\mathbf{F}_d$ (70.1 $\pm$ 4.1 % and 64.4 $\pm$ 17.8 %, respectively), whereas body rotations during the last two wingbeats occurred predominantly about $\mathbf{F}_d$ (60.2 $\pm$ 5.6 % and 69.4 $\pm$ 2.3 %) (Fig. 6C).

In summary, during turning flights the pigeon's torso oscillated vigorously due to the combined effect of the flapping wings (resulting from inertial forces) and aerodynamic forces in relation to gravity. Aerodynamic forces accelerating the bird's center of mass peaked during downstroke, but also peaked during upstroke and were roughly half the downstroke magnitude. These aerodynamic forces serve to offset gravity and change the bird's flight trajectory to achieve level 90° turns. Even though the pigeon's orientation changed significantly about all three body-axes, downstroke-

199 averaged aerodynamic forces were produced in a uniform anatomical direction.
200 Decomposition of successive wingbeat 3D body rotations revealed that early in the turn
201 body rotations of the pigeon mainly redirected downstroke-averaged aerodynamic forces,
202 reflecting anatomical constraints on the direction of aerodynamic force production.
203 However, later in the turn body rotations mainly served to reorient the bird's body for
204 straight flight, and had little effect on the direction of aerodynamic force production.
205
206 **DISCUSSION.** Using an analytical approach based on high-speed 3D kinematics and
207 detailed body mass distributions, we determined the time-varying net aerodynamic forces
208 produced by slowly flying pigeons as they negotiated 90^{o} level turns (Fig. 2). We
209 identified the tip-reversal upstroke as aerodynamically active (Fig. 2, 4B), indicating its
210 role for increased power production and control of body position. Net aerodynamic forces
211 were produced in a uniform direction within the pigeon's body frame, requiring that
212 changes in flight trajectory be mediated by body rotations that redirect aerodynamic force
213 in the global frame (Fig. 5). Consistent with our hypothesis, the overall turning strategy
214 consisted of force vectoring to change the pigeon's flight trajectory, followed by re-
215 acquisition of the bird's preferred body orientation for forward flight (Fig. 6).
216 Substantial rotations occurred about all three anatomical axes indicating that 1)
217 pigeons are not restricted to a particular anatomical axis to change their body orientation,
218 and 2) body rotations function to redirect net aerodynamic forces as needed to negotiate
219 the turn (Table 1). That body rotations occurred mainly about the birds' roll axis does not
220 necessarily reflect a preference for this axis, but may simply reflect the birds' body

orientation upon entering the turn and the reliance on force vectoring to negotiate the turn.

Net Aerodynamic force magnitude (|**F**|) varied consistently, with minima and maxima occurring at wingbeat phases as predicted by aerodynamic theory (21), across all individuals and trials. The average net aerodynamic force per wingbeat was greater than one BW because turning birds need to accelerate themselves to redirect their flight trajectory, as well as offset their weight due to gravity. The small negative peak in |**F**|, opposing the stroke-averaged aerodynamic force, may well reflect an aerodynamic consequence of strong supination of the wings near the downstroke-upstroke transition (22).

Positive aerodynamic force during the upstroke coincided with wing tip-reversal (Fig. 4B, left silhouette). During an upstroke with tip-reversal, the elbow and wrist are flexed, and the hand-wing is supinated, causing it to be inverted. Elbow and wrist flexion effectively moves the point of wing rotation from the shoulder during the downstroke towards the wrist during the upstroke, facilitating the upward ‘back flick’ of the hand-wing. This tip-reversal mechanism is found in the slow to intermediate flight of birds with relatively pointed wings, as well as some birds with rounded wings (22-24), and bats (10, 25-26). The functional significance of wing tip-reversal has been the subject of debate since the pioneering work of Brown (27), and has been proposed by others in prior studies of avian flight to be aerodynamically active (10, 24-34). Until now, however, aerodynamic force production of the tip-reversal upstroke had not been convincingly demonstrated during vertebrate flight.

243 The consistent force patterns observed here across wingbeats of all three pigeons
244 provide the first definitive evidence for upstroke aerodynamic force production during
245 slow flight in birds larger than hummingbirds (Fig. 2, 4). Useful contributions of an
246 active tip-reversal upstroke to weight support can therefore be expected during other
247 modes of flight where tip-reversal is present, such as hovering, landing and steady slow
248 flight. This is reinforced by the fact that we observed no significant differences in
249 upstroke force patterns across the five wingbeats during which birds entered, executed
250 and left the 90° turn. Aerodynamic force generation by the tip-reversal mechanism also
251 agrees with recent force measurements of pigeon wings spun like a propeller, while
252 positioned in an upstroke configuration (35).
253 Although maximum **F** during the upstroke reached 50% of maximum **F** during the
254 downstroke (Fig. 4), the upstroke generated only 27 $\pm$ 4% of the downstroke impulse.
255 The smaller impulse of the upstroke reflects its shorter period (42% of the wingbeat
256 duration), as well as the opposing aerodynamic force production relative to weight
257 support early in the upstroke (Fig. 4B).
258 In a comparative context, the relative contribution of upstroke aerodynamic force
259 to total impulse in pigeons is nevertheless surprisingly high. Hummingbirds operate at
260 temporal and spatial scales similar to insects (2), and, until recently, were thought to
261 share weight support between the two halves of the wingbeat (36). However, hovering
262 rufous hummingbirds generate only 33% of the downstroke impulse during upstroke
263 ((37), based on wake measurements). With an upstroke that generates 27% of their
264 downstroke impulse, pigeons achieve a similar impulse distribution to that found in

rufous hummingbirds, which is remarkable since hummingbirds are thought to have evolved a highly derived upstroke (38).

Our hypothesis that pigeons produce aerodynamic forces in a uniform anatomical direction is also clearly supported (Fig. 5). $\mathbf{F}_d$ was oriented within the mid-sagittal body plane and directed antero-dorsally, with little variation across successive turning wingbeats. Thus, during low speed flight, pigeons exhibit a consistent direction of net aerodynamic force production with respect to their body, reflecting the fundamental anatomical features that underlie powered avian flapping flight.

The constrained direction of force production in the body frame indicates that pigeons turn much like insects and helicopters. Helicopters redirect aerodynamic forces relative to their fuselage (in the body frame) within relatively narrow ranges (roughly 20°; (39)), meaning that maneuvers with more substantial redirections of resultant forces in the global frame require force vectoring, as we found for pigeons. Airplanes, with decoupled wing lift and engine thrust, can redirect resultant forces to a larger degree within the body frame, particularly in the fore-aft direction (for modern fighter planes this can be > 90° (40)), reducing their reliance on force vectoring to maneuver.

The turning strategy of pigeons appears to prioritize trajectory changes over readjustments of body orientation. Body rotations of the pigeons early in the turn mainly contribute to changes in flight trajectory, whereas body rotations progressively later in the turn predominantly serve to realign the body for subsequent forward flight, having a smaller effect on redirecting aerodynamic force (Fig. 6C). This turning strategy likely arises from constraint of $\mathbf{F}_d$ direction with respect to the bird's body, which requires force vectoring to redirect $\mathbf{F}_d$. However, body rotations that redirect $\mathbf{F}_d$ during the first

288 part of the turn result in a body orientation that is not well suited for the bird's new flight
289 trajectory. Therefore, once the bird achieves its new target flight trajectory, its preferred
290 body orientation for forward flight must be reacquired by rotating its body about $\mathbf{F}_d$.
291 Only body rotations that occur about $\mathbf{F}_d$ leave the newly acquired flight trajectory
292 unaffected, which explains why these body rotations predominantly occur later in the
293 turn.

294 To the extent that aerodynamic force production may be anatomically constrained
295 in avian flapping flight, it seems likely that the pattern of early flight trajectory
296 adjustment followed by reacquisition of a preferred forward flight body orientation
297 observed here for slow turning flight may also apply for fast turning flight. At higher
298 flight speeds, however, changes in wings and/or tail configurations are likely to produce
299 more substantial changes in aerodynamic force with respect to the bird's body (41),
300 allowing for changes in aerodynamic force direction, independent of force vectoring, to
301 achieve a turn. Additionally, given that flight power requirements are lowest at
302 intermediate speeds (42), birds may be able to redirect aerodynamic force within the body
303 frame by differentially activating flight muscles between their inside and outside wings.
304 This could enable an alternative turning strategy to that observed here. For instance,
305 during flight versus when flap-running, chukars produced aerodynamic forces roughly in
306 the same global direction, yet body pitch orientation differs by about 30° between these
307 behaviors (43). These findings indicate that birds may be able to re-direct aerodynamic
308 forces more variably with respect to the body depending on behavior or power output.

309 At the low flight speeds examined here, pigeons operate much like helicopters,
310 which have limited capacity to redirect aerodynamic forces relative to their body, relying

311 on whole-body force vectoring to change flight trajectory, similar to fruit flies, blow flies
312 and house flies (5, 7, 44, 45). The moderate redirection of $\mathbf{F}_d$ with respect to the pigeon's
313 body that does occur, may contribute to body torques required to produce the body
314 rotations needed for turning (11,12). Understanding flight control will therefore require
315 insight into the specific mechanisms used by pigeons to generate the torques that produce
316 the observed body rotations. However, torques cannot be inferred from Newton's second
317 law of motion because the distribution of applied forces remains unknown. Nevertheless,
318 by limiting the direction of aerodynamic force production to a single main axis relative to
319 the body, our results indicate that birds may simplify the problem of controlling turns
320 from six to four degrees of freedom (46).
321
322 **METHODS.** Three rock doves (*Columba livia*) were selected from ten wild-caught
323 individuals, based on subjective assessment of their initial turning flight performance
324 during training. These pigeons were housed, trained and studied at the Concord Field
325 Station (Bedford, MA, USA) in accordance with protocols approved by Harvard
326 University's Institutional Animal Care and Use Committee. The pigeons were trained to
327 fly back and forth between two perches situated at either end of two 5m long by 1m wide
328 by 2m high netted sections, connected by a 90º turn midway (Fig. 2B). The symmetrical,
329 square-corner corridor was constructed of lightweight, 2-cm mesh nylon deer netting
330 supported by a PVC frame consisting of 4-cm diameter piping.
331 Using nine synchronized, high-speed cameras, 3D positions of body markers were
332 collected within a calibrated 1.8 m^3 cubic volume that encompassed the turn. Trials
333 accepted for analysis were those in which the birds 1) did not contact the netting, and 2)

maintained a turning flight trajectory relative to global horizontal of < 5°. The pigeons were marked at 16 anatomical locations (Fig. 3): Dorsum at the second thoracic vertebra (dm); Left and right rump (4-cm lateral to the vertebral column over the synsacrum) (ru); Center of head (hd); Left and right wing roots (sh); Left and right wrists (wr); Tip of left and right 5^{th} primary feathers (5p); 67% of the length of left and right 9^{th} primary feathers (9p); 67% along the length of left and right outer tail feathers (tl); Left and right tip of the innermost secondary feathers (1s). Elbow position was determined trigonometrically based on two lengths and three positions: brachial and ante- brachial segment lengths and wing root, wrist and tip of the innermost secondary feather positions. Flights were recorded with two camera systems: A high-speed light video system recording at 250 Hz with 0.001 sec exposure time, consisting of one FastCam-X 1280 PCI and two FastCam 1024 PCI cameras (Photron USA Inc., San Diego, CA, USA), and an infrared-based auto-tracking system recording at 240 Hz with 0.0004 sec exposure time, consisting of six ProReflex MCU240 cameras (Qualisys AB, Gothenburg, Sweden), was used to track flight kinematics. The two camera systems were synchronized using a start trigger signal. The visible-light videos were digitized using DLTdv3 (47). Calculations were performed in Matlab (Mathworks Inc., Natick, MA) using custom-written scripts. Positional data were filtered with a fourth-order Butterworth filter using a low-pass cutoff frequency three times the wingbeat frequency. Cutoff frequency was determined by residual analysis (48).

Rotations. The sum of absolute back and forth rotations within a wingbeat and the net change in body orientation over a wingbeat period were defined as continuous and net wingbeat body rotations, respectively, about each of the body axes. For each turn, five

sequential wingbeats were analyzed, during which continuous and net wingbeat body rotations about each axis were accumulated.

Aerodynamic Forces. The position of the net CM was approximated throughout the turn using a mass-distribution model of the body and tail, head, and wings (Fig. 3). The torso and tail were represented by a single point-mass, because the effect of tail movements on net CM were assumed to be minor and are difficult to model. The head and 14 chord-wise strips per wing were modeled as point-masses, with time-varying positions based on segment kinematics (Fig. 3). The two wings together constitute approximately $1/8^{th}$ of a pigeon's body mass. The motion of the flapping wings causes the net CM to move substantially relative to a pigeon's torso CM, necessitating the time-dependent, non-body-fixed CM calculations.

Wingbeats were partitioned into upstroke and downstroke phases, based on reversal of the major bending direction of the primary feathers. This bending-reversal of the primary feathers coincided with the instant the primary feather markers moved laterally relative to the body, in both ventral (start of upstroke) and dorsal (start of downstroke) positions.

Instantaneous net aerodynamic forces (**F**) were determined throughout the turn based on net CM accelerations relative to gravity, because the CM of a freely flying bird can only be accelerated by external gravitational and aerodynamic forces. **F** vectors were normalized to wingbeat phase and expressed in the body frame. The net aerodynamic forces averaged over the duration of the downstroke ($\mathbf{F}_{d)}$ act in line with the main impulse vector, the time integral of force, produced during each wingbeat.

Redirection of aerodynamic forces versus rotation about aerodynamic forces. Identification of $\mathbf{F}_d$ allowed for decomposition of body rotations relative to this direction of main aerodynamic impulse imparted during each downstroke. Body rotations of the bird were analyzed with respect to $\mathbf{F}_d$ over the five wingbeats of the turn. Two 3D rotations were calculated between successive mid-downstroke instants of each wingbeat: a 3D body rotation and a 3D redirection of $\mathbf{F}_d$. Body rotations identical to the redirection of $\mathbf{F}_d$ were designated as representing 100% redirection of $\mathbf{F}_d$. Conversely, if body rotations did not redirect $\mathbf{F}_d$, body rotations were designated as representing 100% rotation about $\mathbf{F}_d$. Mathematically, this approach is identical to expressing the 3D body rotation as a vector in the body frame and determining the relative magnitudes of two perpendicular projections of this vector: 1) The projection of the 3D body rotation vector on the plane normal to $\mathbf{F}_d$ represents the component of the body rotation that redirects $\mathbf{F}_d$ (force vectoring), and 2) The projection of the 3D body rotation vector on $\mathbf{F}_d$ represents the component of the body rotation about $\mathbf{F}_d$. This approach allowed any 3D body rotation to be decomposed into two complementary body rotation fractions, one that redirected $\mathbf{F}_d$ and one that rotated about $\mathbf{F}_d$ (Fig. 6A,B).

Statistics. All results were are based on five complete wingbeats nearest the center of each of two left and two right turns for each individual (20 wingbeats per bird, N=3) expressed as mean $\pm$ SD. Paired t-tests (JMP, SAS Institute, Cary, NC) were used to compare group means for the three individuals. Differences were considered significant when $p<0.05$.

ACKNOWLEDGMENTS. We thank P.A. Ramirez for care of the animals, D.E. Lieberman for shared use of the Qualysis cameras, and A.N. Ahn, D.R. Warrick, A.S. Arnold-Rife, C.A. Moreno, T.E. Higgins, A. Eberle, C. Gastil, and A. Randall for helpful discussions and informal contributions to this work. We furthermore thank three anonymous reviewers for their constructive suggestions. This research was funded by NSF IOS-0744056 to AAB.

FOOTNOTES.

Specific author contributions. A.A.B. and I.G.R. designed research. I.G.R and A.A.B performed research. I.G.R., L.C.B., M.A.B. and A.N.P. analyzed data. I.G.R. and A.A.B. wrote the paper.

REFERENCES.

1. Arbib MA, Érdi P & Szentágothai J (1997) *Neural Organization: Structure, Function, and Dynamics*, Cambridge, MA: Bradford Book/MIT.

2. Dudley R (2000) *The Biomechanics of Insect Flight. Form, Function, Evolution* (Princeton University Press, Princeton).

3. Stepniewski WZ & Keys CN (1984) *Rotary-wing Aerodynamics* (Dover Publications, New York).

4. Blondeau J (1981) Aerodynamic capabilities of flies, as revealed by a new technique. J Exp Biol 92: 155-163.

5. Götz KG, Wandel U (1984) Optomotor control of force and light in *Drosophila* and *Musca*, II Covariance of lift and thrust in still air. Biol Cyb 51: 135–139.

6. Sugiura H & Dickinson MH (2009) The generation of forces and moments during visually-evoked steering maneuvers in flying *Drosophila*. PLoS ONE 4: e4883.

7. Wagner H (1986) Flight performance and visual control of flight of the freeflying housefly (*Musca domestica* L.). I. Organization of the flight motor. Phil Trans R Soc Lond B 312: 527-551.

8. Collett TS & Land MF (1975) Visual control of flight behaviour in the hoverfly, *Syritta pipiens* L. J Comp Physiol A 99: 1–66.

9. Nachtigall W (1979). Schiebeflug bei der Schmeißfliege *Calliphora erythrocephala* (Diptera: Calliphoridae). Entom Gen 5: 255–265.

10. Aldridge HDJN (1986) Kinematics and aerodynamics of the Greater Horseshoe Bat (*Rhinolopus ferrumequinum*) in horizontal flight at various flight speeds. J Exp Biol 126: 479–497.

446 11. Warrick DR & Dial KP (1998) Kinematic, aerodynamic and anatomical mechanisms
447 in the slow, maneuvering flight of pigeons. J Exp Biol 201: 655-672.
448
449 12. Hedrick TL & Biewener AA (2007) Low speed maneuvering flight of the rose-
450 breasted cockatoo (*Eolophus roseicapillus*). I. Kinematic and neuromuscular control of
451 turning. J Exp Biol 210: 1897-1911.
452
453 13. Iriarte-Diaz J & Swartz SM (2008) Kinematics of slow turn maneuvering in
454 the fruit bat *Cynopterus brachyotis* J Exp Biol 211: 3478-3489.
455
456 14. Berg AM & Biewener AA (2010) Wing and body kinematics of takeoff and landing
457 flight in the pigeon (*Columba livia*) J Exp Biol 213: 1651-1658.
458
459 15. Sy M (1936) Funktionell-anatomische Untersuchungen am Vogelflügel. Journal für
460 Ornithologie 84: 199–296.
461
462 16. Rayner JMV (1988) The evolution of vertebrate flight. Biol J Linn Soc 34: 269–287.
463
464 17. Dial KP, Goslow GE & Jenkins FA (1991) The functional anatomy of the shoulder in
465 the European starling (*Sturnus vulgaris*). J Morphol 207: 327–344.
466
467 18. Gatesy SM & Baier DB (2010) The origin of the avian flight stroke: a kinematic and
468 kinetic perspective. Paleobiology 31: 382-399.

19. Phillips WF (2004) *Mechanics of Flight* (Wiley, Hoboken).

20. Biewener AA, Corning WR & Tobalske BW (1998) *In vivo* pectoralis muscle force–length behavior during level flight in pigeons (*Columba livia*). J Exp Biol 201: 3293–3307.

21. Greenewalt CH (1975) The Flight of Birds: The Significant Dimensions, Their Departure from the Requirements for Dimensional Similarity, and the Effect on Flight Aerodynamics of That Departure. Transactions of the American Philosophical Society, 65: 1-67.

22. Brown RHJ (1963) The flight of birds. Biol Rev 38: 460-489.

23. Zimmer K (1943) Der Flug des Nektarvogels (*Cinnyris*). Journ F Orn 91: 371-387.

24. Tobalske BW (2007) Biomechanics of bird flight. J Exp Biol 210: 3135–3146.

25. Norberg UM (1976) Aerodynamics, kinematics, and energetics of horizontal flapping flight in the long-eared bat *Plecotus auritus*. J Exp Biol 65: 179-212.

26. Norberg UM (1990) *Vertebrate flight* (Springer-Verlag, Berlin).

27. Brown RHJ (1948) The flapping cycle of the pigeon. J Exp Biol 25: 322-333.

28. Alexander R McN (1986) *Animal Mechanics*, Seattle: Univ. Wash. Press.

29. Azuma A (1992) *The Biokinetics of Flying and Swimming*, New York: Springer.

30. Bundle MW & Dial KP (2003) Mechanics of wing-assisted incline running (WAIR). J Exp Biol 206: 4553-4564.

31. Hedrick TL, Usherwood JR & Biewener AA (2004) Wing inertia and whole-body acceleration: an analysis of instantaneous aerodynamic force production in cockatiels (*Nymphicus hollandicus*) flying across a range of speeds. J Exp Biol 207: 1689-1702.

32. Iriarte-Diaz J, Riskin DK, Willis DJ, Breuer KS & Swartz SM (2011) Whole-body kinematics of a fruit bat reveal the influence of wing inertia on body accelerations. J Exp Biol 214: 1546-1553.

33. Lorenz KZ (1933) Beobachtetes über das Fliegen der Vögel und über die Beziehungen der Flügel- und Steuerform zur Art des Fluges. Journal für Ornithologie 81: 107–236.

34. Spedding GR, Rayner JMV & Pennycuick CJ (1984) Momentum and energy in the wake of a pigeon (*Columba livia*) in slow flight. J Exp Biol 111: 81-102.

35. Crandell KE & Tobalske BW (2011) Aerodynamics of tip-reversal upstroke in a revolving pigeon wing. J Exp Biol 214: 1867-1873.

36. Weis-Fogh T (1972) Energetics of hovering flight in hummingbirds and in *Drosophila*. J Exp Biol 56: 79-104.

37. Warrick DR, Tobalske BW & Powers DR (2005) Aerodynamics of the hovering hummingbird. Nature 435: 1094-1097.

38. Stolpe M & Zimmer K (1939) Der Schwirrflug des Kolibri im Zeitlupenfilm. J Orn 87: 136-155.

39. Talbot PD & Corliss LD (1977) A Mathematical force and moment model of a UH-1H helicopter for flight dynamics simulations NASA Ames Research Center and Ames Directorate, USAAMRDL, AVRAD-COM.

40. Winchester J (2006) *The Encyclopedia of modern aircraft: from civilian airliners to military superfighters* (Thunder Bay Press, San Diego).

41. Rüppell G (1977) *Bird flight* (Von Nostrand Reinhold, New York).

42. Tobalske BW, Hedrick TL, Dial KP & Biewener AA (2003) Comparative power curves in bird flight. Nature 421: 363-366.

43. Dial KP, Jackson BE & Segre P (2008) A fundamental avian wing-stroke provides a new perspective on the evolution of flight. Nature 451: 985-990.

44. Fry SN, Sayaman R & Dickinson MH (2003) The Aerodynamics of Free-Flight Maneuvers in *Drosophila*. Science 300: 495-498.

45. Vogel S (1966). Flight in *Drosophila*. I. Flight performance of tethered flies. J Exp Biol 44: 567-78.

46. LaValle SM (2006) *Planning algorithms* (Cambridge Univ. Press, Cambridge).

47. Hedrick TL (2008) Software techniques for two- and three-dimensional kinematic measurements of biological and biomimetic systems. Bioinspiration Biomimetics 3: 034 001.

48. Winter DA (2005) *Biomechanics and Motor Control of Human Movement* (Wiley, Hoboken).

Figure Legends.

559 Fig. 1. Schematic representation of the experimental hypotheses. The global frame (thin
560 grey lines) with z (vertical) defined in line with gravity, and x and y defined along the
561 two perpendicular horizontal axes of the flight corridor (Fig. 2). Upper right inset: The
562 bird's body frame with antero-posterior (along the spine), medio-lateral and dorso-ventral
563 axes in red, green and blue, respectively. Rotations about these anatomical axes are
564 defined as roll, pitch and yaw (red, green and blue circular arrows). (A, B) Hypothetical
565 aerodynamic forces (solid light blue vectors) in the global frame (thin solid grey lines)
566 during a level, 90° aerial turn to the right. Horizontal and vertical global projections
567 (dashed blue vectors) of the aerodynamic forces early, during and upon completion of the
568 turn provide braking, centripetal and accelerating forces, respectively, as well as vertical
569 forces. (A) $H_{0:}$ Birds produce aerodynamic forces in variable directions in the body
570 frame, requiring only realignment of the antero-posterior body axis with the flight
571 trajectory. (B) Force-vectoring Hypothesis: Birds produce aerodynamic forces in a
572 uniform direction in the body frame, requiring body rotations to redirect aerodynamic
573 forces in the global frame to change flight trajectory (grey curved line). NB: the grey
574 triangles shown between the antero-posterior body axis and resultant aerodynamic force
575 vector are of identical dimensions in each of the four represented positions of the turn,
576 emphasizing the anatomically fixed direction of aerodynamic force.
577
578 Fig. 2. Instantaneous net aerodynamic forces (**F**) visualized on corresponding center of
579 mass (CM) positions throughout a representative right 90^{o} turn. Downstroke forces in
580 blue and upstroke forces in red, plotted at 4 ms intervals. (A-C) **F** in the global frame
581 with axes x, y and z. (A) Top view. (B) Schematic of the flight corridor with viewpoints

582 for (A) and (C). (C) Level view. (D) Caudo-lateral view of **F** for a single wingbeat in the
583 body frame with antero-posterior (ap, red), medio-lateral (ml, green) and dorso-ventral
584 (dv, blue) axes. Arrows connecting vector tips indicate temporal sequence. (A,C,D) Axes
585 lengths represent two body weights of force.
586
587 Fig. 3. Pigeon marker locations and mass-distribution model. Silhouette at mid
588 downstroke with sixteen marker locations (solid black circles) and calculated elbow
589 locations (open circles). The approximate wingstrip edges (dashed lines) and marker
590 descriptors are provided for the bird's right side (dm: dorsal midshaft; ru: rump; sh:
591 shoulder, 5p: fifth primary; 9p: ninth primary; tl: tail; 1s: innermost secondary; see
592 methods for details). Modeled point masses (blue spheres), with size representing relative
593 mass. Note that the tail is considered part of the torso mass (largest blue sphere).
594
595 Fig. 4. Net aerodynamic force magnitude (|**F**|) in line with the stroke averaged
596 aerodynamic force for turning pigeons. The force magnitude is normalized to body
597 weight (BW) and wingbeat duration. Grey shading indicates downstroke. (A) Mean |**F**| $\pm$
598 SD (N=20) for each of 3 individual pigeons. (B) Pooled mean $\pm$ SD of the mean |**F**|
599 across the three pigeons. Representative silhouette at both phases of upstroke and
600 downstroke peak force (black arrows) illustrates timing with respect to wing
601 configuration. Note that the discontinuity between upstroke and downstroke traces results
602 from normalization to the half-stroke phases, necessitated by variations in stroke
603 durations.
604

Fig. 5. Mean net downstroke aerodynamic forces ($\mathbf{F}_d$) for three turning pigeons expressed in the body frame and superimposed on a pigeon outline. The mean $\pm$ SD vector cone is depicted by a different color for each individual averaged for all analyzed wingbeats of the turns. For clarity, three views are provided. (A) rear view, (B) side view and (C) oblique view.

Fig. 6. Decomposition of sequential body rotations of a turning pigeon. (A,B) Outline of a pigeon, with superimposed $\mathbf{F}_d$ and SD vector cone, as well as the plane to which $\mathbf{F}_d$ is normal, and an exemplary axis of body rotation (thick black line), all in the body frame. (A) The component of the body rotation that redirects $\mathbf{F}_d$ (blue circular arrow). Note that the axis describing this rotation fraction lies within the circular blue plane. (B) The component of the body rotation about $\mathbf{F}_d$ (orange circular arrow). (C) Fractions of body rotation for four sequential, complete wingbeats of the turn, showing the orthogonal components of body rotations that redirect $\mathbf{F}_d$ (blue fraction) versus which occur about $\mathbf{F}_d$ (orange fraction). Pooled mean $\pm$ SD of means of three individuals. Mid-downstroke outlines of five sequential wingbeats, as seen from a single elevated viewpoint from inside the turn. Grey arrows and dotted lines link colored bars to positions in the turn. Asterisks indicate significant differences between body rotation fractions.

Table Legend.

Table 1. Body rotations accumulated throughout the turn. Mean $\pm$ SD of means of three individuals for both continuous and net wingbeat effects in terms of roll, pitch and yaw.

A. Body-independent force redirection

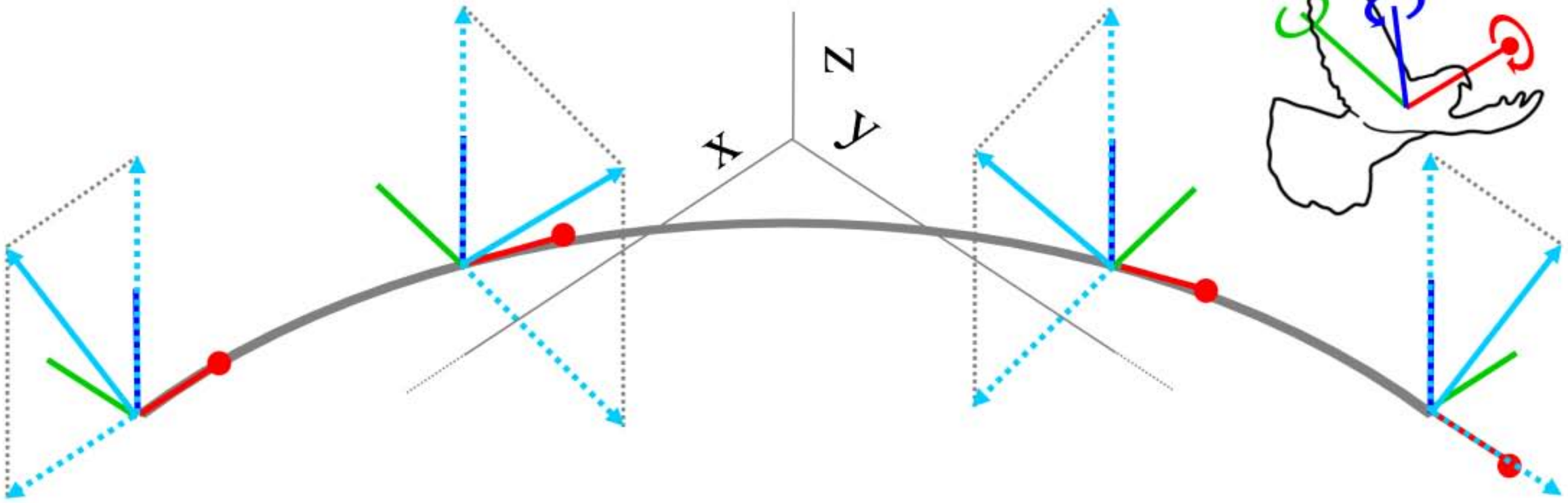

B. Force vectoring through body rotations

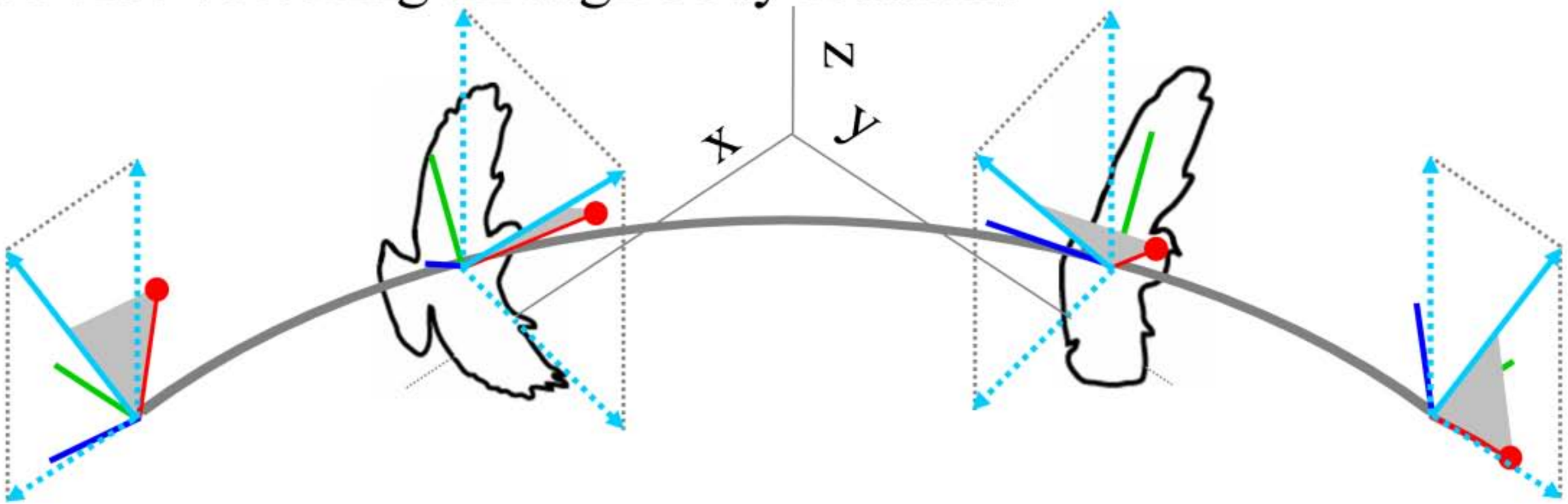

A

X Y

Top view

B

z

x

2 m

1 m

5 m

y

dv

ml

ap

C

Level view

Z

X Y

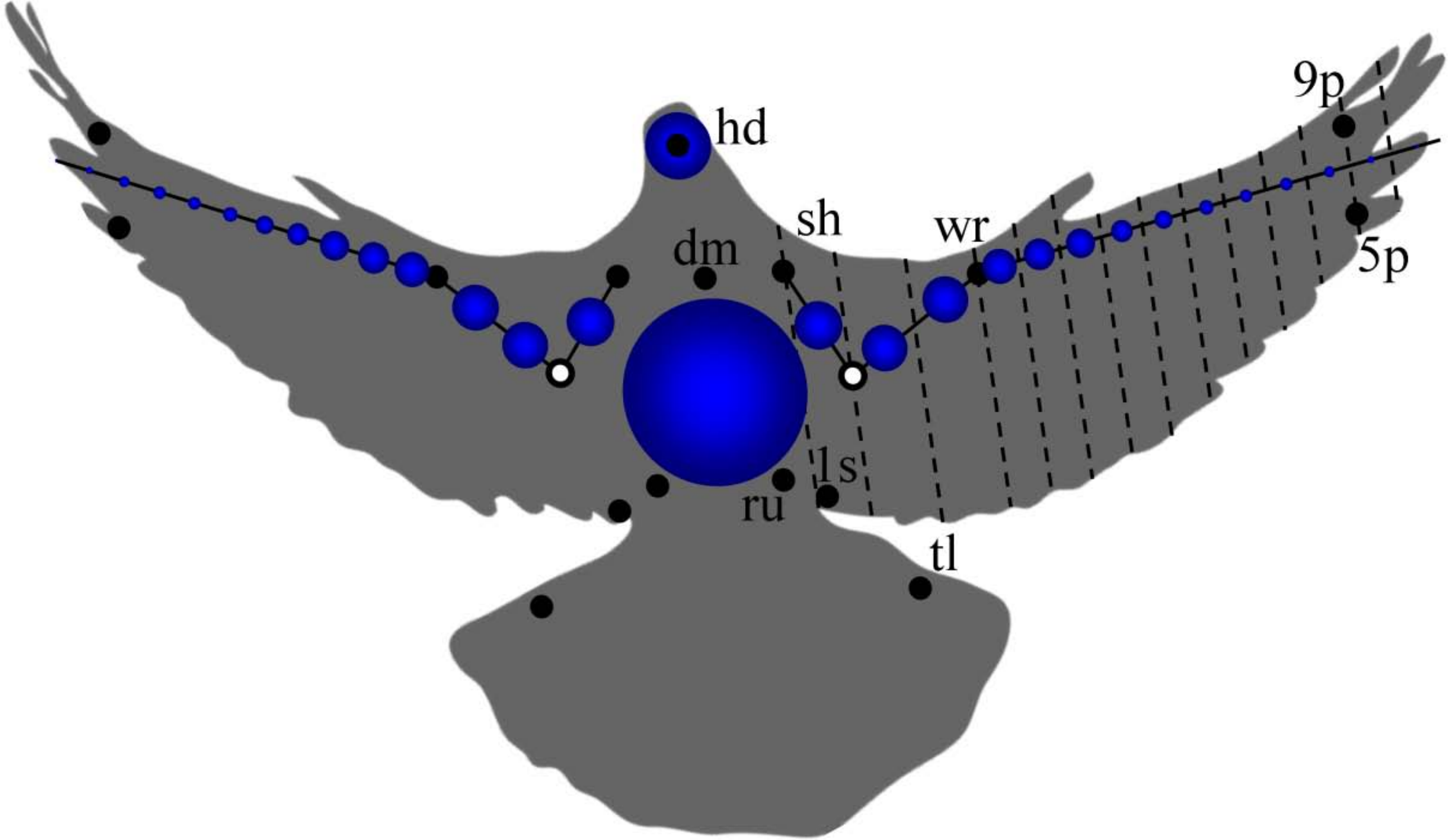
hd
dm
sh
wr
9p
5p
ls
ru
tl

A

Force (BW)

4

0

0 0.42 1 0 0.42 1 0 0.43 1

Wingbeat phase

B

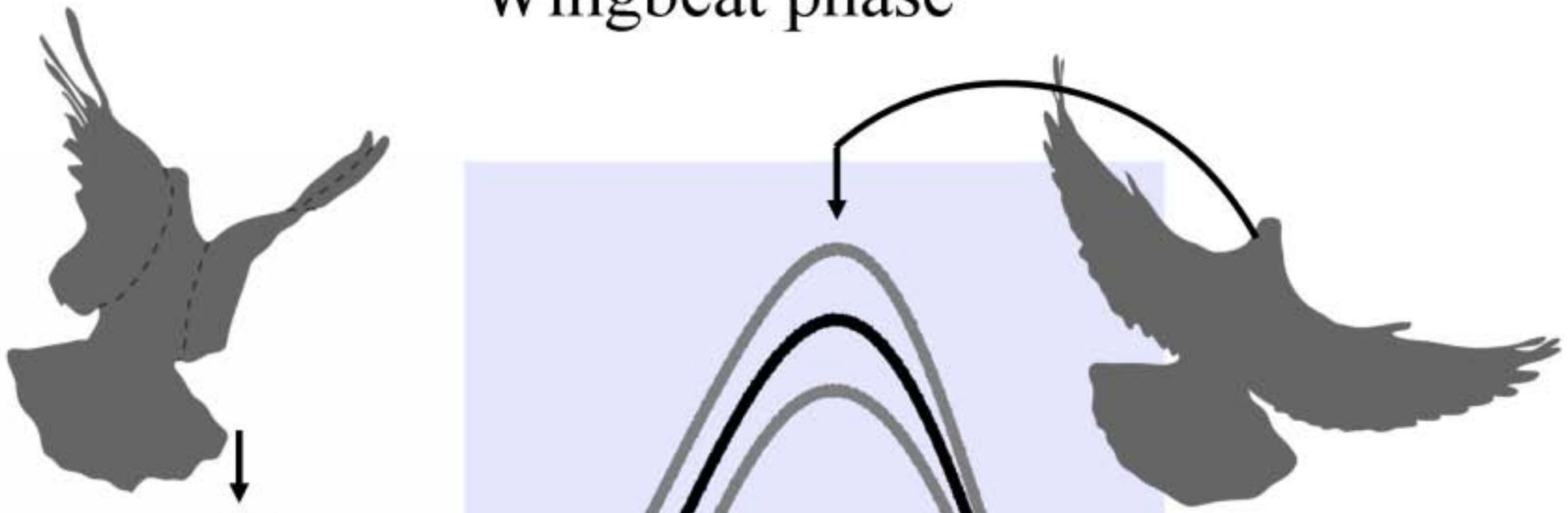

Force (BW)

4

0

0 0.42 1

Wingbeat phase

A

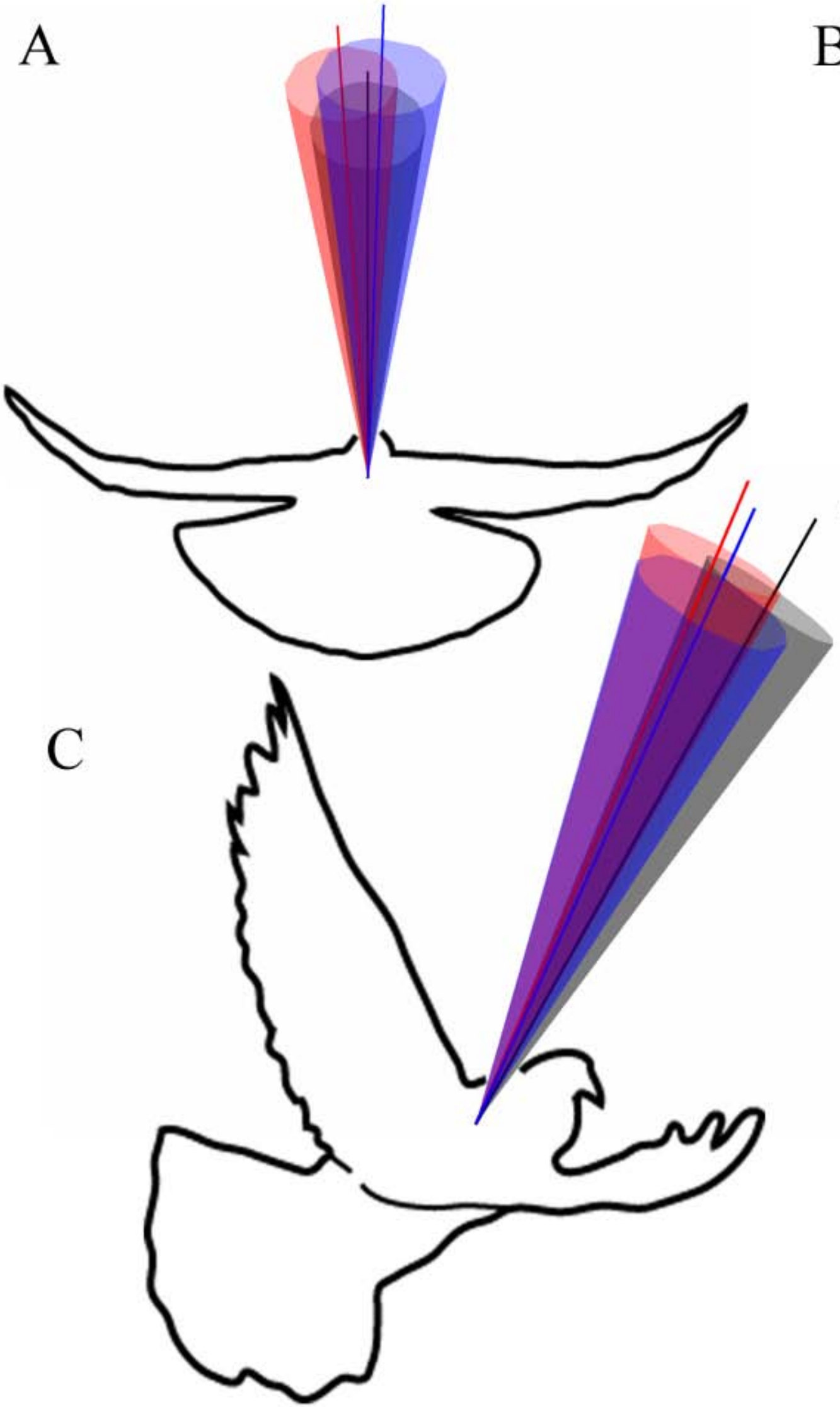

B

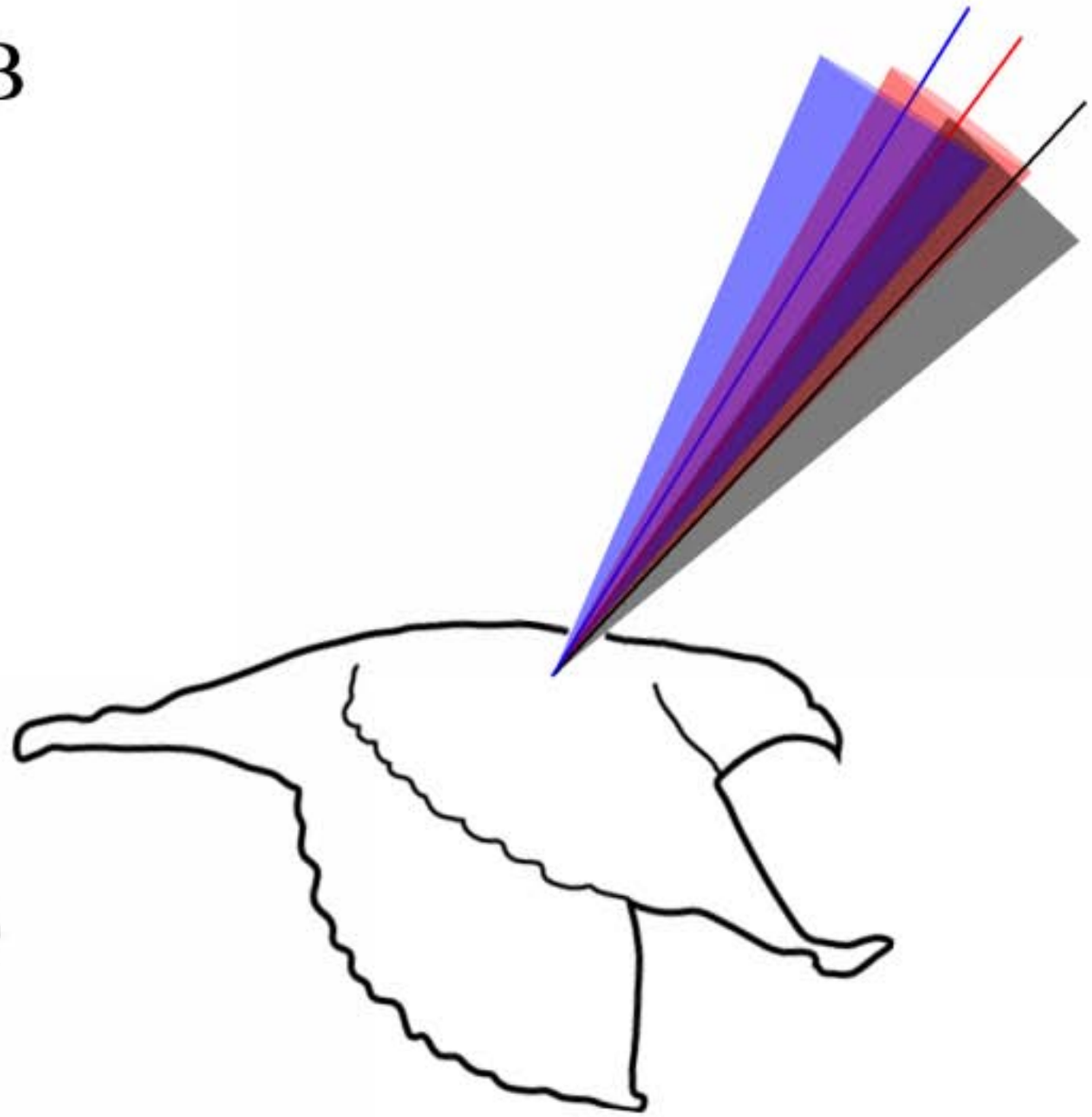

C

A

B

C

100

0

Body rotation fraction (%)

*

*

*

Body rotations	Continuous effects (deg)	Net wingbeat effects (deg)
Roll	143 ± 16	77 ± 14
Pitch	125 ± 24	43 ± 2
Yaw	81 ± 10	58 ± 4